Excitons in near-surface quantum wells in magnetic fields: Experiment and theory

N. A. Gippius,[a),b)] A. L. Yablonskii, A. B. Dzyubenko, and S. G. Tikhodeev
General Physics Institute, Russian Academy of Sciences, 117942 Moscow, Russia

L. V. Kulik and V. D. Kulakovskii
Institute of Solid State Physics, Russian Academy of Sciences, 142432 Chernogolovka, Russia

A. Forchel
Technische Physik, Universität Würzburg, D-97074 Würzburg, Germany

(Received 5 January 1998; accepted for publication 6 February 1998)

The exciton transition and binding energies have been investigated in near-surface InGaAs/GaAs quantum wells theoretically and experimentally (by photoluminescence and photoluminescence excitation spectroscopy at 4.2 K). The contribution induced by vacuum has been analyzed for the ground and excited exciton states in perpendicular magnetic fields up to 14 T. The vacuum potential barrier has been shown to increase the magnetoexciton transition energies, $\hbar\omega_n$, but nearly not to influence their binding energies, E_n. In contrast, the image charges (caused by the abrupt, one order of magnitude, decrease of the dielectric constant at the semiconductor-vacuum interface) modify the Coulomb interaction and lead to the increase of both $\hbar\omega_n$ and E_n. The magnetic field has been found to enhance the contribution of the image charges to the exciton binding energy and to decrease their influence on the transition energy. The effect is due to the in-plane exciton wave function squeezing in a magnetic field. © *1998 American Institute of Physics.* [S0021-8979(98)01910-0]

I. INTRODUCTION

It has been predicted[1,2] that excitons in narrow semiconductor layers surrounded by a dielectric of a smaller dielectric constant have to be significantly enhanced. This effect originates from the modification of the electron-hole (e-h) interaction by the images induced by the interfaces between materials with different dielectric constants. This effect is referred to as the dielectric enhancement of excitons. It has been extensively discussed theoretically,[3–7] whereas the experimental study of this effect has met a problem of a fabrication of suitable very narrow (of a few nm) semiconductor layers in the dielectric environment. The experimental study of the exciton dielectric enhancement has been undertaken in thin CdTe films on a dielectric substrate,[8] in self-organized PbI based semiconductor/insulator superlattices, quantum wells (QWs), wires, and dots,[9] and in near surface InGaAs/GaAs quantum wells (NSQWs), i.e., InGaAs QWs separated from vacuum by a thin (3–20 nm) GaAs cap (barrier) layer.[10,11] However, very complicated absorption spectra, measured in Ref. 8, and small (only of the order of few interatomic distances) exciton sizes in PbI based structures,[9] did not allow one to carry out systematic studies of the exciton dielectric enhancement in such semiconductor-insulator structures. Up to date the most promising structures for detailed experimental investigation of the exciton dielectric enhancement seem to be the NSQWs. First, a well developed technique of growing and etching of InGaAs/GaAs QW structures allows one to fabricate such structures with well defined both InGaAs QW and GaAs cap layer thicknesses. Second, both the ground and excited exciton state energies can be measured in available high quality structures with an accuracy providing a quantitative comparison with theoretical calculations. Third, the excitons in these structures are large in comparison to a lattice constant and can be quantitatively described in the Wannier–Mott approximation. In addition, for more detailed studies of the exciton dielectric confinement in such structures,one can apply an external magnetic field. The magnetic field modifies the effective e-h interaction via the change of the exciton wave functions and thereby opens new possibilities to study the dielectric confinement effect in detail.

In the present article we have carried out a systematic experimental and theoretical study of the effect of image charges on the exciton properties in the InGaAS/GaAs NSQWs with cap layer thickness, $L_{\mathrm{cap}}=3$–20 nm. The theory of NSQWs excitons has been developed allowing to calculate the ground and excited exciton energies with and without taking into account image charges at the semiconductor-vacuum (SV) interface both for zero and nonzero magnetic fields. This theory includes the previously considered limits of zero[10] and strong[11] magnetic fields, and it is able to describe the intermediate magnetic field regime. In this work we have considered s- as well as p-excitonic states, and studied the effect of a near-surface perpendicular electric field. The exciton transition energies for the ground and several excited states have been measured in a wide range of magnetic fields $B=0-14$ T with the use of the photoluminescence excitation (PLE) technique. Finally, we have

a)Present address: Technische Physik, Universität Würzburg, D-97074 Würzburg, Germany.
b)Electronic mail: gippius@wpfx32.physik.uni-wuerzburg.de

analyzed the observed evolution of the *s*-exciton transition energies with increasing magnetic field and decreasing cap layer thickness. Such an analysis has allowed us to separate the effect on *s*-excitonic states of the high vacuum potential barrier from that of the image charges and to carry out the detailed study of the dielectric enhancement effect.

The article is organized as follows. In Sec. II the theoretical model for magnetoexcitons in NSQWs is presented. In Sec. III the experimental methods are described. In Sec. IV we present the theoretical and experimental data and their comparison.

II. THEORY

A. Model equations

We consider strained InGaAs NSQWs with GaAs barriers. The light–heavy hole splitting in such QWs is strongly enhanced due to the strain (see, e.g., Ref. 12), therefore we can neglect the split-off light-hole band and consider only heavy-hole magnetoexcitons in a rather wide range of energies. In this approximation, the NSQW electron-hole Hamiltonian in the magnetic field $\mathbf{B}=(0,0,B)$ takes the form

$$H=H_{\rm ez}+H_{\rm hz}+H_{\rm 2D}+U_{\rm eh}\equiv H_0+U_{\rm eh}. \tag{1}$$

Here

$$H_{\rm jz}=-\frac{\hbar^2}{2m_{\rm jz}}\frac{\partial^2}{\partial z_j^2}+V_j(z_j)+V_{\rm self}(z_j),\quad j=e,h. \tag{2}$$

The band-offset potentials are $V_j=\infty$ $(j=e,h)$ in vacuum $(z<0)$, V_e and V_h inside the InGaAs QW $(L_{\rm cap}<z<L_{\rm cap}+L_{\rm QW})$, and $V_j=0$ in the barrier GaAs layers, $m_{\rm ez}$ and $m_{\rm hz}$ are the electron and heavy hole effective masses, respectively. The potential

$$V_{\rm self}(z)=\frac{e^2}{2\epsilon}\left(\frac{\epsilon-1}{\epsilon+1}\right)\frac{1}{2|z|}, \tag{3}$$

(where ϵ is the dielectric constant of the semiconductor) takes into account the repulsion of the charge from its self-image; we neglect a small difference between ϵ in $In_xGa_{1-x}As$ and GaAs. This approach can be modified to account for an electric field along the z axis, $\mathscr{E}=(0,0,\mathscr{E})$, by additional terms in Eq. (2), $+(-)e\mathscr{E}z_e(h)$.

Hamiltonian $H_{\rm 2D}$ describes the two-dimensional (2D) motion of a free e-h pair in the magnetic field

$$H_{\rm 2D}=\frac{1}{2m_{e\|}}\left(-i\hbar\nabla_{\rho_e}+\frac{e}{c}\mathbf{A}_e\right)^2+\frac{1}{2m_{h\|}}\left(-i\hbar\nabla_{\rho_h}-\frac{e}{c}\mathbf{A}_h\right)^2, \tag{4}$$

where $\mathbf{A}_j=\frac{1}{2}\mathbf{B}\times\boldsymbol{\rho}_j$ is the vector potential in the symmetric gauge, $\boldsymbol{\rho}=\boldsymbol{\rho}_e-\boldsymbol{\rho}_h=(x,y)$, and $\mathbf{r}_j=(\boldsymbol{\rho}_j,z_j)$. We neglect also a small mass difference in the well and barrier layers. The potential

$$U_{\rm eh}(\rho,z_e,z_h)=-\frac{e^2}{\epsilon}\left[\frac{1}{\sqrt{\rho^2+(z_e-z_h)^2}}+\frac{\epsilon-1}{\epsilon+1}\frac{1}{\sqrt{\rho^2+(z_e+z_h)^2}}\right] \tag{5}$$

takes into account, in addition to the Coulomb interaction between the electron and hole, the attraction of the electron to the hole image, and of the hole to the electron image.

In order to solve the quantum-mechanical problem of the magnetoexciton in a NSQW, one can diagonalize numerically the matrix of the Coulomb potential (5) on the basis of noninteracting two-particle states of Hamiltonian H_0. Such an approach, when the expansion is performed in Landau levels (LLs), has been used previously in the problem of quasi-two-dimensional excitons in coupled double QWs[13] in a magnetic field (see also Ref. 14).

Assuming a strong vertical quantization in the QW potentials $V_j(z_j)$, $j=e,h$, the wave functions of optically active $\mathbf{K}=0$ s excitons (with the angular momentum projection of the relative e-h motion $l_z=0$) take the form

$$\Psi_{\mathbf{K}=0,s}(\mathbf{r}_e,\mathbf{r}_h)=\exp\left(\frac{i[\boldsymbol{\rho}\times\mathbf{R}]_z}{2l_B^2}\right)\zeta_1(z_e)\xi_1(z_h)\times\sum_n A_n^{(s)}\phi_{nn}(\rho), \tag{6}$$

where $\mathbf{K}$ is the conserved magnetic center-of-mass momentum,[15,16] ζ_1 and ξ_1 are the ground state eigenfunctions of Hamiltonians $H_{\rm ez}$ and $H_{\rm hz}$, respectively, $l_B=(\hbar c/eB)^{1/2}$ is the magnetic length, $\mathbf{R}=(m_{e\|}\boldsymbol{\rho}_e+m_{h\|}\boldsymbol{\rho}_h)/M$, $M=m_{e\|}+m_{h\|}$

$$\phi_{n\,n}(\rho)=\frac{1}{(2\pi l_B^2)^{1/2}}L_n\left(\frac{\rho^2}{2l_B^2}\right)\exp\left(-\frac{\rho^2}{4l_B^2}\right)$$

and $L_n(x)$ is the Laguerre polynomial, $n=0,1,\ldots$.

As the experiments show (see Sec. III), additional transitions are resolved, which can be ascribed to nominally optically inactive $2p^{\pm}$ heavy-hole excitons (see Sec. IV below). The wave functions of, e.g., $\mathbf{K}=0$ $p^{\pm}$ excitons (with $l_z=\pm1$) can be written in forms similar to Eq. (6) (see also Ref. 17)

$$\Psi_{\mathbf{K}=0,p^+}(\mathbf{r}_e,\mathbf{r}_h)=\exp\left(\frac{i[\boldsymbol{\rho}\times\mathbf{R}]_z}{2l_B^2}\right)\zeta_1(z_e)\xi_1(z_h)\times\sum_n A_n^{(p^+)}\phi_{n+1\,n}(\boldsymbol{\rho}), \tag{7}$$

$$\Psi_{\mathbf{K}=0,p^-}(\mathbf{r}_e,\mathbf{r}_h)=\exp\left(\frac{i[\boldsymbol{\rho}\times\mathbf{R}]_z}{2l_B^2}\right)\zeta_1(z_e)\xi_1(z_h)\times\sum_n A_n^{(p^-)}\phi_{n\,n+1}(\boldsymbol{\rho}), \tag{8}$$

where

$$\phi_{n+1\,n}(\boldsymbol{\rho}) = \phi_{n\,n+1}(\boldsymbol{\rho})^* = \frac{1}{(2\pi l_B^2 2[n+1])^{1/2}}\left[\frac{x+iy}{l_B}\right]L_n^1\left(\frac{\rho^2}{2l_B^2}\right) \times \exp\left(-\frac{\rho^2}{4l_B^2}\right),$$

$\phi_{n\,n'}(\boldsymbol{\rho})$ are the factored wave functions in a magnetic field, the quantum numbers n and n' correspond to the electron and hole Landau level numbers, respectively; the angular momentum projection $l_z = n - n'$.

The expansion in Landau levels converges rapidly in high magnetic fields $l_B/a_{Be(h)} < 1[a_{Be(h)} = \epsilon\hbar^2/m_{e(h)\|}e^2]$. In the limit $l_B/a_{Be(h)} \ll 1$, the $l_z = 0$ excitonic states labeled (using the 2D hydrogenic notations) ns, $n = 1,2,...$, are predominantly formed by the orbital $\phi_{n-1n-1}(\boldsymbol{\rho})$ in the $n-1$ electron and hole Landau levels. Similarly, the $l_z = \pm 1$ excitonic states labeled np^+ [and np^-] are formed predominantly by the orbitals $\phi_{n\,n-1}(\boldsymbol{\rho})$ [and $\phi_{n-1\,n}(\boldsymbol{\rho})$, respectively], i.e., in the $n[n-1]$ electron and $n-1[n]$ hole Landau levels. At low magnetic fields, a number of other Landau levels are admixed due to the Coulomb e-h interaction. Taking into account of up to 36 Landau level orbitals $\phi_{n\,n'}(\boldsymbol{\rho})$, we have numerically treated in Ref. 11 the problem of magnetoexcitons in InGaAs/GaAs NSQWs with reasonable accuracy at $B > 3$ T.

Such an approach cannot be used at lower magnetic fields, because the number of Landau levels to be taken into account to achieve the needed accuracy increases rapidly.[14] In the regime of strong QW confinement, it is possible to overcome this difficulty. Indeed, the Schrödinger equation for the $\mathbf{K} = 0$ exciton wave function, after averaging of Hamiltonian Eq. (1) over the quantum confined electron and hole eigenfunctions in the z direction, is reduced to an effectively one-dimensional (ID) equation

$$H_\rho \psi_{n,l_z}(\boldsymbol{\rho}) = E_{n,l_z}\psi_{n,l_z}(\boldsymbol{\rho}), \psi_{n,l_z}(\boldsymbol{\rho}) = \exp(i\varphi l_z)\phi_{n,l_z}(\rho), \tag{9}$$

$$H_\rho = -\frac{\hbar^2}{2\mu}\nabla_\rho^2 + \frac{e^2B^2}{8\mu c^2}\rho^2 + \frac{e\hbar B}{2c}\left(\frac{1}{m_e} - \frac{1}{m_{h\|}}\right)\hat{l}_z + V(\rho), \tag{10}$$

$$V(\rho) = \int dz_e \int dz_h U_{\mathrm{eh}}(\rho, z_e, z_h)\zeta_1^2(z_e)\xi_1^2(z_h), \tag{11}$$

[where $\mu = (1/m_e + 1/m_{h\|})^{-1}$ is the reduced exciton mass], which can be easily integrated numerically. The generalization of this procedure to a multilevel situation (e.g., for several QW levels or for coupled double or triple QWs) will be presented elsewhere.[18]

This approach (the numerical solution of the in-plane magnetoexciton Schrödinger equation) produces the same results (with absolute accuracy better than 0.1 meV) for the $1s,\ldots 4s$ exciton binding energies as the previously reported approaches in zero[10] and in quantizing[11] magnetic fields. It is also applicable in the intermediate magnetic fields. Thus, within the framework of the single approach it is possible to calculate the evolution of the exciton states in the whole range of magnetic fields.

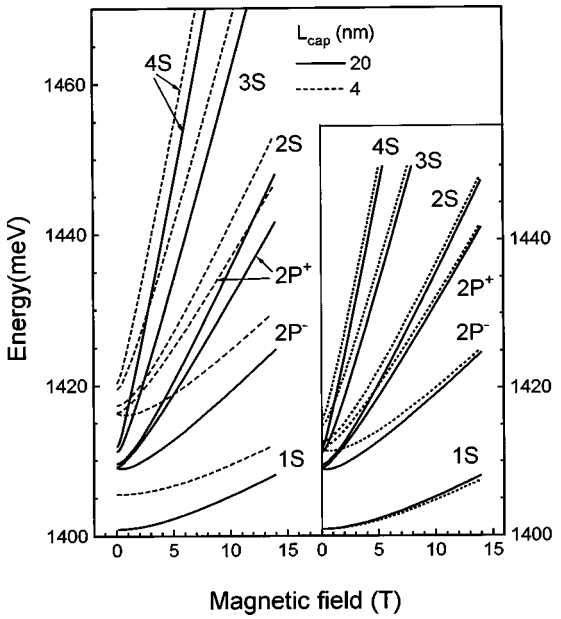

FIG. 1. Landau fan diagrams of the NSQW magnetoexciton, calculated for $L_{\mathrm{cap}} = 20$ and 4 nm (solid and dashed lines, respectively). Dashed-dotted lines in the inset are a redshifted fan diagram for $L_{\mathrm{cap}} = 5$ nm so that the $1s$ transition energy coincides with that for $L_{\mathrm{cap}} = 20$ nm.

B. Magnetoexciton transition and binding energies

The calculated magnetoexciton transition energies of the lowest s and p states, $\hbar\omega_{\mathrm{ns}}$ and $\hbar\omega_{\mathrm{np}}$, take the form of well known fan diagrams and are illustrated in Fig. 1. The numerical calculations were carried out for $L_{\mathrm{QW}} = 5$ nm $In_{0.18}Ga_{0.82}As/GaAs$ NSQWs, using the following parameters: $V_e = -113$ meV and $V_h = -75$ meV, $m_{\mathrm{ez}} = m_{e\|} = 0.067$, $m_{\mathrm{hz}} = 0.35$, $m_{h\|} = 0.2$, and $\epsilon = 12.5$. Left panel in Fig. 1 displays the fans, calculated for two cap layer thicknesses, $L_{\mathrm{cap}} = 20$ and 4 nm, at zero electric field $\mathscr{E} = 0$. Note a small energy splitting between the $2s$, $2p^{\pm}$ states at $B = 0$, which is a consequence of the non-Coulombic form of the effective 2D exciton interaction, Eq. (11).

It is seen that the decrease of the cap layer thickness causes a strong blueshift of all transition energies, $\hbar\omega_n$. The blueshift increases with the level number, n, and decreases with increasing magnetic field. These changes can be seen better in the inset of Fig. 1, where we have shifted the calculated Landau fan for $L_{\mathrm{cap}} = 4$ nm QW so that its $1s$ transition energy at $B = 0$ coincides with that for $L_{\mathrm{cap}} = 20$ nm QW.

The blueshift of magnetoexciton levels with decreasing L_{cap} is due to two different reasons. The first one is the influence of the high vacuum potential barrier in a close vicinity of the QW. This barrier causes an additional (to the QW) localization of electrons and holes. Hence, it enhances the free electron and free hole energies with the decrease of L_{cap}.[19] This effect has a tunneling origin; we will call it a ''tunneling blueshift.''

The second reason for the blueshift is the *repulsion* between charges and their self-images, accounted for by the term V_{self}, Eq. (3). We will call this component of the shift a ''dielectric blueshift.'' For an electrically neutral exciton, the dielectric blueshift is partly compensated by the *attraction*

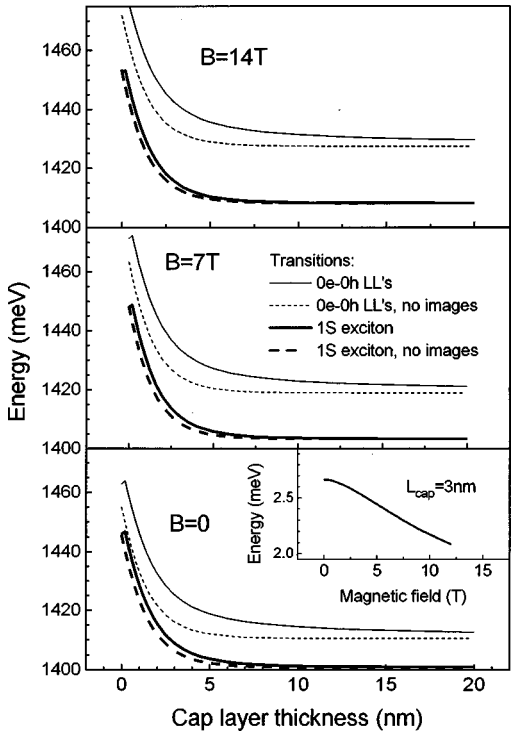

FIG. 2. Dependences of the $1s$ transition energies, $\hbar\omega_{1s}$ and $\hbar\omega_{1s,0}$, on the cap layer thickness, $L_{\rm cap}$, calculated with and without accounting for the interaction with images (thick solid and dashed lines, respectively), at $B=0$, 7 and 14 T. Corresponding dependences of energy splittings between zero free electron and hole Landau levels (LLs), $\hbar\omega_{00}$ (of band gap in the case of $B=0$), are shown by thin solid and dashed lines. The inset displays the magnetic field dependence of the dielectric blueshift, $\hbar\omega_{1s}-\hbar\omega_{1s,0}$, calculated for $L_{\rm cap}=3$ nm.

between the hole (electron) and the electron (hole) image [the second term in Eq. (5)]. This attraction is just the exciton dielectric enhancement. It enhances the exciton binding energies and thus reduces magnetoexciton blueshift with the decrease of $L_{\rm cap}$.

Figure 2 shows the calculated dependences of $\hbar\omega_{1s}$ (thick solid curves), in comparison with the dependences of the energy gap between zero Landau levels of the noninteracting electron and hole, $\hbar\omega_{00}$ (thin solid curves), for $B=0$, 7, and 14 T at $\mathscr{E}=0$. To distinguish between the tunneling and dielectric parts of the blueshift of the $1s$ state, we display in Fig. 2 as well the dependences $\hbar\omega_{1s}$ and $\hbar\omega_{00}$ (thick and thin dashed lines, respectively), calculated without the terms, responsible for the interaction with the image charges, i.e., Eq. (3) and the second term in Eq. (5). Physically, the corresponding Hamiltonian describes a system where vacuum is replaced by a dielectric with infinite interface potential barriers, but with the same dielectric constant as in the semiconductor.

The difference between magnetoexciton transition energies $\hbar\omega_{1s}$, calculated with and without accounting for image charges, is much smaller than that for $\hbar\omega_{00}$. Moreover, as the inset at the bottom panel of Fig. 2 shows, this difference decreases with B at a fixed $L_{\rm cap}$. Thus, the $1s$ transition energy blueshift has mainly the tunneling origin, and its small dielectric counterpart is further decreased with the increase of the magnetic field.

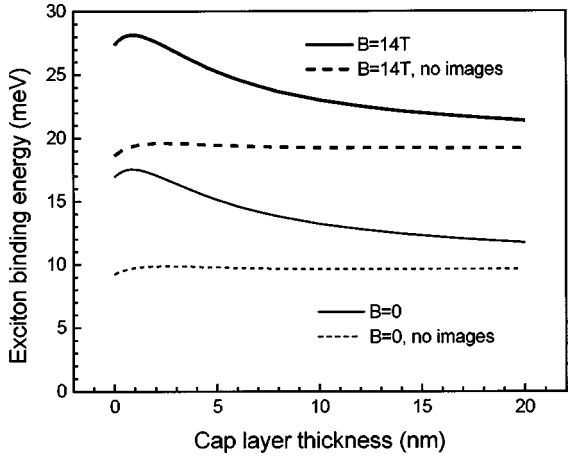

FIG. 3. Dependences of $1s$ exciton binding energies, $E_{1s}=\hbar\omega_{00}-\hbar\omega_{1s}$, on $L_{\rm cap}$, calculated with and without accounting for the interaction with images (solid and dashed lines, respectively), at $B=0$ and 14 T (thin and thick lines, respectively).

Figure 3 compares the dielectric enhancement of binding energy, $E_{1s}=|\hbar\omega_{00}-\hbar\omega_{1s}|$, in the range of $L_{\rm cap}=2$–20 nm at $B=0$ and 14 T (thin and thick solid lines, respectively). In addition to a well known increase of E_{1s} in a magnetic field, Fig. 3 shows as well that E_{1s} increases strongly with approaching of the QW to vacuum.[20] The latter dependence is completely due to interaction with images. The calculated E_{1s} without allowing for image charges (shown in Fig. 3 by dashed curves) does not depend markedly on $L_{\rm cap}$.

Thus the calculations show that the tunneling effect influences very weakly the exciton binding energy, but it causes a large $1s$ transition energy blueshift. In contrast, the dielectric effect is responsible for the exciton enhancement, but changes weakly $1s$ transition energy. Such a behavior originates from the exciton electroneutrality. The smaller the in-plane size of the magnetoexciton, the better is the cancelling (in the exciton transition energy) of the dielectric blueshift of $\hbar\omega_{00}$ by the redshift due to the enhanced binding energy. The squeezing of magnetoexcitons in a magnetic field reduces the blueshift of exciton levels as shown in the inset in Fig. 2. As expected, the change of the transition energy due to the dielectric effect is larger for higher, more extended, magnetoexciton states. These effects are clearly seen in Fig. 1, right panel. Thus, to measure the dielectric confinement effect, the evolution of inter-level splittings, $\Delta_{n'n}=E_{n's}-E_{ns}$ rather than the interband transition energies has to be investigated.

One more reason why the investigation of inter-level magnetoexciton splittings is preferable is connected to an influence of the surface charge induced electric field, which may exist in NSQWs (see, e.g., Ref. 21). The latter effect increases when the QW approaches vacuum. We have calculated the influence of the electric field on the magnetoexciton transition energies in NSQWs with strong vertical confinement, and have found that the perpendicular electric field $\mathscr{E}=(0,0,\mathscr{E})$ causes nearly the same Stark shifts of all lower-lying magnetoexciton levels. This is illustrated in Fig. 4, where the change of the transition energies $E_{ns}-E_{ns}|_{\mathscr{E}=0}$, $n=1,2,3,4$ (top panel) and of the magnetoexciton level split-

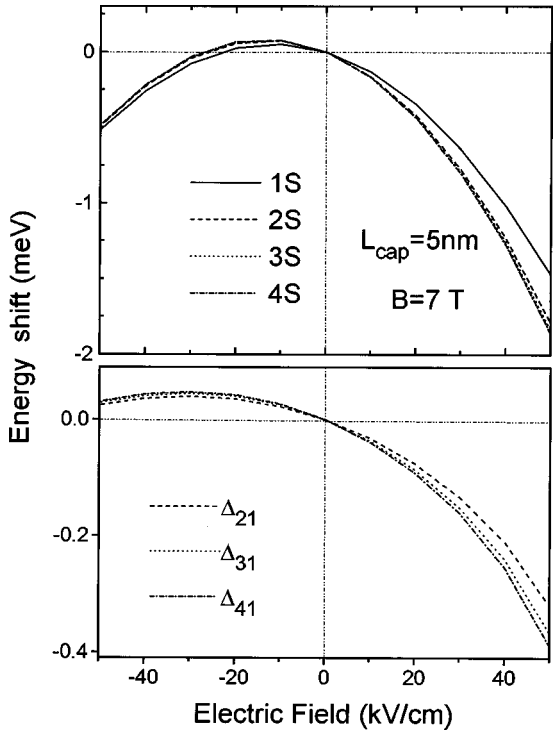

FIG. 4. Calculated Stark shift of the magnetoexciton transition energies, $\hbar\omega_{ns}-\hbar\omega_{ns}|_{\mathscr{E}=0}$, $n=1,2,3,4$ (top), and the change of the inter-level splittings, $\Delta_{n1}-\Delta_{n1}|_{\mathscr{E}=0}$, $n=2,3,4$ (bottom), at $B=7$ T and $L_{\mathrm{cap}}=5$ nm.

tings $\Delta_{n1}-\Delta_{n1}|_{\mathscr{E}=0}$, $n=2,3,4$ (bottom panel) is shown as a function of the electric field $\mathscr{E}$ up to ± 50 kV/cm (which corresponds to the SV interface charge density of $\approx \pm 3 \times 10^{11}$ cm^{-2}). Figure 4 shows that the Stark shift of transition energies is nearly one order of magnitude larger than the change of the inter-level splittings. This is not surprising because the electric field directly influences the QW confined levels, whereas the effective in-plane e-h interaction in the QW exciton is changed only through the modification of the QW wave functions $\zeta_1(z_e)$, $\zeta_1(z_h)$.

For a QW in the bulk, the Stark shift is quadratic in $\mathscr{E}$, because the exciton wave function has a definite parity under inversion $z\rightarrow -z$. In an NSQW this symmetry is broken, and the Stark effect becomes linear in a weak electric field as shown in Fig. 4, because of nonzero dipole moment of the exciton in a NSQW, directed from the NSQW into the bulk. The effect depends on L_{cap}, and in principle can be used for experimental investigation of the magnitude and direction of the near-surface electric field.

Physically, this dipole moment appears because of repulsion of the electron and hole from their self-images, and as a consequence of electron and hole mass difference: heavier holes localize inside a NSQW under this repulsion at a larger distance from the SV interface. (Note that without accounting for images, a tunneling effect causes nonzero exciton dipole moment of the *opposite* direction, from QW towards the SV interface, because of vacuum barrier pushing out of lighter electrons.)

Under a negative electric field (see Fig. 4), which corresponds to a negative net charge on the SV interface, the exciton dipole moment decreases. It comes through zero at some magnitude of the electric field. Under positive electric fields (when the SV interface has a positive net charge), the exciton dipole moment grows up.

III. EXPERIMENT

A. Experimental setup

For the measurements we have chosen strained $In_xGa_{1-x}As/GaAs$ heterostructures with $x\sim 0.18$ and a QW thickness $L_{\mathrm{QW}}=5$ nm. At this thickness, there is only one bound state in the conduction band. A stress induced splitting of the valence band in the InGaAs layer exceeds 40 meV.[12] Therefore any spectral features in this energy range are related to the excited states of the heavy-hole exciton ($2s$, etc). The additional advantages of such QW structures are (i) a strong (one order of magnitude) decrease of ϵ at the SV interface, and (ii) a large exciton radius ($a_B\sim 80$ Å). An as grown sample with $L_{\mathrm{cap}}=20$ nm was used as a reference. After measuring photoluminescence (PL) and photoluminescence excitation (PLE) spectra, the cap layer was thinned by etching. Two problems have to be solved in the etching process, namely, one has to avoid surface defects and to avoid cap layer thickness fluctuations (after the etching). For example, fluctuations of only about 2 ML at $L_{\mathrm{cap}}=3$ nm result in such a strong emission line broadening that PLE spectroscopy becomes impossible. We have used dry etching by an Ar^+-ion beam to remove the cap layer gradually. To avoid defect formation, low (500 eV) ion energy, low sample temperature (liquid nitrogen), and a small angle between the ion beam and the sample surface (20°) have been used.[22]

Both PL and PLE spectra were recorded with the use of a Ti-sapphire laser and a double grating monochromator RAMANOR U1000 at 4.2 K. The sample was located in a helium cryostat with superconducting solenoid. The emission of the NSQW was excited and collected via the same quartz fiber with a diameter of 0.6 mm located just near (0.2 mm) the sample surface. A cooled photomultiplier in the photon counting mode has been used for the detection of the PL.

B. PL and PLE spectra of the NSQW

Typical PL and PLE exciton spectra are displayed (by dashed and solid curves, respectively) in Fig. 5 for NSQWs with $L_{\mathrm{cap}}=20$, 5, and 3 nm and at several magnetic fields $B\leqslant 14$ T. Figures show that the etching of the cap layer results in a relatively small exciton line broadening indicating a high surface quality. The PL spectrum consists of a single line corresponding to the recombination of excitons in the ground state. At zero magnetic field the PLE spectra show two peaks associated with the $1s$ and $2s$ exciton transitions. The small shift of the $1s$ exciton peak of about 1.5 meV to higher energies in comparison to its energy in the PL spectrum is connected with exciton localization effects.[23] The spectral shifts of the $1s$ exciton line in the PL and PLE spectra for different cap layer thicknesses are very similar which indicates a rather weak increase of localization effects with decreased L_{cap}.

With increasing magnetic field the lines $1s$ and $2s$ move to higher energies. At $B>3$ T, we resolve new lines which correspond to the higher ns magnetoexciton states. Also, at

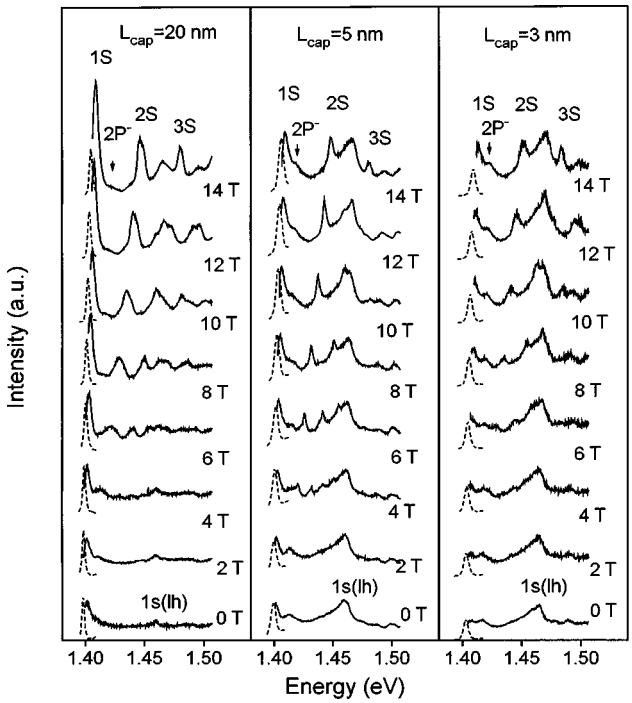

FIG. 5. PL (dashed lines) and PLE (solid lines) magnetoexciton spectra, measured in NSQWs with $L_{cap}=20$, 5, and 3 nm.

high fields two additional weak lines become resolved in the spectral range between the $1s$ and $2s$ states. These lines seem to be due to the emission of $2p^{\pm}$ heavy-hole excitons (see Sec. IV). Figure 5 shows that the intensity of these lines is very weak in the initial QW with 20-nm-thick cap layer but increases strongly with cap layer etching.

The PLE spectra in Fig. 5 allow us to measure the magnetoexciton transition energies in the ground and excited states at different L_{cap}. We will discuss these data and compare it with the theoretical results in the next section.

IV. DIELECTRIC ENHANCEMENT OF EXCITONS: RESULTS AND DISCUSSION

The transition energies measured in the NSQW with the subsequent etching of the cap layer are displayed in Fig. 6 for $L_{cap}=20$, 5, and 3 nm as functions of the magnetic field. The decrease of L_{cap} does not qualitatively change the behavior of exciton transition energies. This is in agreement with the calculations (see Sec. II B above). For all transitions, the blueshift increases with reducing cap layer thickness at any fixed magnetic field.

Comparison of experiment and calculations in Fig. 6 shows that the blueshift is smaller than calculated at $\mathscr{E}=0$ by several meV for NSQWs with smaller $L_{cap}=5$ and 3 nm. (Dotted curves in Fig. 6 show the $1s$ and $2s$ transition energies, calculated for smaller cap thicknesses in vanishing electric field.) This disagreement can be removed if we suppose that at small L_{cap} the QW is influenced by an electric field induced by the surface charge. The calculated Landau fans for the NSQWs with $L_{cap}=20$ nm ($\mathscr{E}=0$) and with $L_{cap}=5$ and 3 nm ($\mathscr{E}=50$ kV/cm) are shown in Fig. 6 by solid lines. They are in good agreement with the experiment. The field $\mathscr{E}=50$ kV/cm corresponds to a positive surface charge density $\sim 3\times 10^{11}\,|e|/\mathrm{cm}^2$. This magnitude and direction of the electric field are consistent with those obtained in Ref. 21.

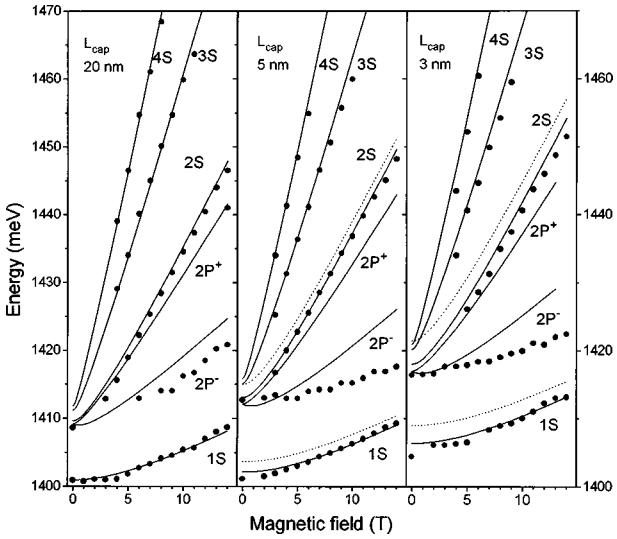

FIG. 6. Measured (dots) and calculated (solid lines) Landau fan diagrams for magnetoexcitons in NSQWs with $L_{cap}=20$, 5, and 3 nm. The theoretical curves for $L_{cap}=5$ and 3 nm are calculated for the electric field $\mathscr{E}=+50$ kV/cm, corresponding to a positive charge on the SV interface $\approx 3\times 10^{11}\,e/cm^2$. The dotted curves (in the central and right panels) show the positions of the $1s$ and $2s$ levels in vanishing electric field.

However, the difference between the measured and calculated at $\mathscr{E}=0$ blueshift can be ascribed as well to an error in the measurements of the cap layer thickness. Figure 7, right panel, demonstrates that the experimental results for the

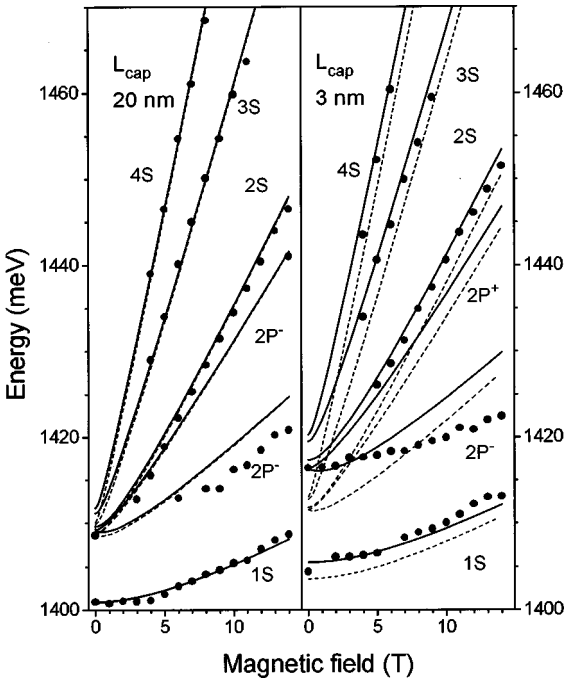

FIG. 7. Measured and calculated Landau fan diagrams for magnetoexcitons in NSQWs with $L_{cap}=20$ nm (left panel). Measured Landau fan diagrams for magnetoexcitons in NSQWs with $L_{cap}=3$ nm, and calculated fans for $L_{cap}=4$ nm (right panel). The theoretical curves are calculated with and without accounting for interaction with images (solid and dashed lines, respectively).

NSQW with $L_{cap}=3$ nm (dots) are well described without any near-surface electric field if one suggests that L_{cap} is 4 rather than 3 nm (solid lines). This is not far from the estimated accuracy in the measurements of L_{cap}. Thus, additional experiments are necessary to prove the role of the near-surface electric field.

In Figs. 6 and 7 the calculated $2p^{\pm}$ exciton transition energies are also shown, in order to compare with the data for additional experimentally resolved lines. These states, which are nominally optically inactive in ideal QWs in the bulk, may become optically active in NSQWs (with inherently broken inversion symmetry), due to the admixture of light hole $1s$-exciton components in the same lowest NSQW subbands. Such light hole-heavy hole exciton mixing in a perpendicular to a QW electric field, which breaks the inversion symmetry, has been considered in Ref. 24. However, only $2p^{-}$ state may contain such an admixture of the $1s$ light hole component.

Another possible reason may be the axial symmetry breaking presumably caused by the cap layer thickness fluctuations and/or in-plane components of the near-surface electric field. This mechanism makes both the $2p^{-}$ as well as $2p^{+}$ transitions. Figure 5 shows that the intensity of these lines is very weak in the initial QW with 20-nm-thick cap layer but increases strongly with cap layer etching. This enhancement may be caused by the increasing influence of the SV interface roughness.

From Figs. 6 and 7 it is seen that the theoretical $2p^{\pm}$ curves do not describe the experimental data for the additional lines in high magnetic fields. An increased (with the decreasing L_{cap}) discrepancy for dipole forbidden optical transitions for p states can be connected with the fact that these transitions become allowed probably due to scattering on the fluctuations of the SV surface and hence occur at $\mathbf{K}\neq 0$. Note that the p magnetoexcitons have negative dispersion.[25] Therefore the difference between the experiment and calculations for p states in Figs. 6 and 7 could be partly due to the neglected mixing of states with a finite $\mathbf{K}$.

However, the most striking feature of the observed exciton spectra for smaller cap layers (see Figs. 6 and 7) is that the splitting between the $2p^{-}$ and $1s$ states decreases *in high magnetic field* with increasing B. Theoretically, this splitting should increase with B as

$$\frac{e\hbar B}{m_{h\|}c}+E_{1s}(B)-E_{2p^{-}}(B).$$

For example, for a strictly 2D magnetoexciton in the high magnetic field limit[25]

$$E_{1s}(B)=\sqrt{\frac{\pi}{2}}\frac{e^2}{\epsilon l_B}\equiv E_0\sim\sqrt{B},\quad E_{2p^{-}}(B)=0.5E_0.$$

At the present moment this discrepancy is not understood.

We turn now to the discussion of the dielectric confinement effect. The effect increases with the reducing L_{cap}. This is seen from the comparison between left and right panels of Fig. 7, where dashed lines show the Landau fan diagrams, calculated without accounting for the interaction with images. The left panel in Fig. 8 displays the measured and

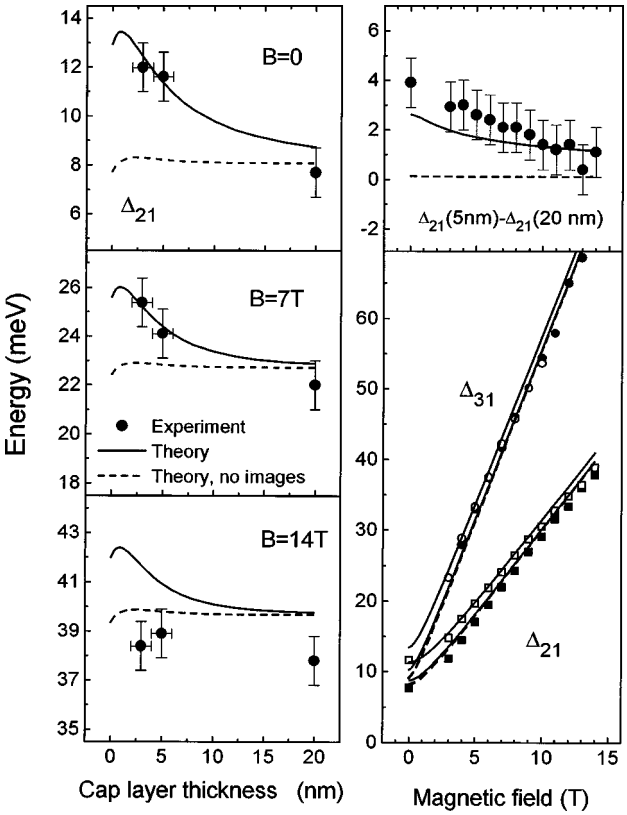

FIG. 8. Measured (dots) and calculated (lines) evolution of $2s-1s$ energy splitting, Δ_{21}, with L_{cap}, at $B=0$, 7, and 14 T (left panel). Solid lines show theory with accounting for images, and dashed lines without images. Measured (dots and boxes) and calculated (lines) evolution of $3s-1s$ and $2s-1s$ energy splitting with B, for $L_{cap}=5$ and 20 nm (right panel, bottom). The experimental data for $L_{cap}=5$ and 20 nm are shown by open and filled symbols, respectively. The evolution of the difference $\Delta_{21}|_{L_{cap}=5\text{ nm}}-\Delta_{21}|_{20\text{ nm}}$ with B is shown in the inset (right panel, top).

calculated dependences of the $2s-1s$ energy splitting, Δ_{21}, as a function of L_{cap} for $B=0$, 7, and 14 T. It can be seen that at 0 and 7 T the measured $2s-1s$ splitting (dots) coincides 14 T. It can be seen that at 0 and 7 T the measured $2s-1s$ splitting (dots) coincides with calculations, allowing for the interaction with images (solid lines). As expected, the splitting increases strongly with the decrease of L_{cap}, and the magnitude of this increase falls down with the magnetic field. The comparison in Fig. 8 of the experimental points with the dashed lines, calculated without accounting for the dielectric confinement effect, shows clearly that the increase of Δ_{21} with reducing L_{cap} has the dielectric origin.

The measured $2s-1s$ splitting at 14 T as well decreases with the increase of L_{cap} in a qualitative agreement with calculations. However, the measured values at 14 T turn out to be markedly smaller than the calculated ones. This quantitative discrepancy seems to be connected with the fact that in our calculations we neglect the heavy-hole–light-hole magnetoexcitons interaction. The contribution from this interaction at 14 T can be essential because the $2s-1s$ splitting becomes close to the splitting of the $1s$ light and heavy-hole excitons (cf. Fig. 5).

Figure 8 also compares the measured and calculated magnetic field dependences of the $3s-1s$ and $2s-1s$ en-

ergy splittings, Δ_{31} and Δ_{21} (right panel, bottom). The experimental values are shown by filled dots and boxes for $L_{\mathrm{cap}}=20$ nm, and by open dots and boxes for $L_{\mathrm{cap}}=5$ nm. The calculated curves are shown by solid and dashed lines for calculations with and without accounting for images, respectively. The dashed curves for NSQWs with $L_{\mathrm{cap}}=5$ and 20 nm coincide because the splitting is nearly independent of L_{cap} if the interaction with images is neglected. In contrast, the experiment demonstrates a well pronounced change of $2s-1s$ splitting with L_{cap}. It is seen that the magnetic field dependence of this splitting is in good agreement with the theoretical predictions when the charge images are taken into account. To illustrate the influence of magnetic field on the effect of the dielectric enhancement, we compare in Fig. 8, right panel (top), the measured and calculated difference of the $2s-1s$ energy splitting between $L_{\mathrm{cap}}=20$ and 5 nm, $\Delta_{21}|_{L_{\mathrm{cap}}=5\ \mathrm{nm}}-\Delta_{21}|_{L_{\mathrm{cap}}=20\ \mathrm{nm}}$, at $B\leqslant 14$ T. The figure shows that this difference falls down with the magnetic field, as discussed in Sec. II B. This effect originates from the in-plane squeezing of the magnetoexciton wave function. Again the calculated curve is in agreement with the experiment.

V. CONCLUSIONS

In conclusion, the magnetoexciton transition energies, binding energies, and wave functions in InGaAs/GaAs near-surface quantum wells have been calculated in low and quantizing magnetic fields with taking into account for vacuum induced modifications of the electron-hole Hamiltonian, namely, (i) a high potential barrier and (ii) the image-charge-caused modification of the Coulomb interaction. The photoluminescence excitation studies of excitons have been used to measure the splitting between the ground and the excited magnetoexciton states in a wide range of magnetic fields as a function of the cap layer thickness. A good quantitative agreement has been found between experiment and theory both for the ground and excited *s* states. This has allowed us to separate the contributions due to the high potential barrier and due to the image-charge-caused modification of the Coulomb interaction and to investigate these contributions in detail. We have demonstrated theoretically and experimentally the strong dielectric enhancement of magnetoexcitons in NSQWs.

ACKNOWLEDGMENTS

The authors would like to thank G. E. W. Bauer, M. Bayer, V. Emiliani, and R. Zimmermann for useful discussions and T. Borzenko and Yu. Koval' for the assistance in the cap layer etching. The work was supported by the Russian Foundation for Basic Research (Grant Nos. 97-02-17538 and 97-02-17600) and the Russian Ministry of Science programs ''Surface Atomic Structures'' and ''Nanostructures.'' N.G. acknowledges the support of the Alexander von Humboldt Foundation.

[1] N. S. Rytova, Dokl. Akad Nauk Arm. SSR **163**, 1118 (1965).
[2] L. V. Keldysh, Pis'ma Zh. Eksp. Teor. Fiz. **29**, 716 (1979) [JETP Lett. **29**, 658 (1979)].
[3] E. Hanamura, N. Nagaosa, M. Kumagai, and T. Takagahara, Mater. Sci. Eng., B **1**, 255 (1988).
[4] D. B. Tran Thoai, R. Zimmermann, M. Grundmann, and D. Bimberg, Phys. Rev. B **42**, 5906 (1990).
[5] E. A. Andryushin and A. P. Silin, Fiz. Tverd. Tela (Leningrad) **35**, 1947 (1993) [Sov. Phys. Solid State **35**, 972 (1993)].
[6] T. Takagahara, Phys. Rev. B **47**, 4569 (1993).
[7] E. A. Muljarov, S. G. Tikhodeev, N. A. Gippius, and T. Ishihara, Phys. Rev. B **51**, 14370 (1995).
[8] N. A. Babaev, V. S. Bagaev, F. V. Garin, A. V. Kochemasov, L. V. Paramonov, N. N. Salaschenko, and V. B. Stopachinskii, Pis'ma Zh. Eksp. Teor. Fiz. **40**, 190 (1984) [JETP Lett. **40**, 952 (1984)].
[9] T. Ishihara, J. Takahashi, and T. Goto, Phys. Rev. B **42**, 11099 (1990); T. Ishihara, J. Lumin. **60,61**, 269 (1994).
[10] L. V. Kulik, V. D. Kulakovskii, M. Bayer, A. Forchel, N. A. Gippius, and S. G. Tikhodeev, Phys. Rev. B **54**, R2335 (1996).
[11] A. L. Yablonskii, A. B. Dzyubenko, S. G. Tikhodeev, L. V. Kulik, and V. D. Kulakovskii, Pis'ma Zh. Eksp. Teor. Fiz. **64**, 47 (1996) [JETP Lett. **64**, 51 (1996)].
[12] J. M. Jerard and J. Y. Marzin, Phys. Rev. B **40**, 6450 (1989).
[13] A. B. Dzyubenko and A. L. Yablonskii, Phys. Rev. B **53**, 16 355 (1996).
[14] C. Stafford and S. Schmitt-Rink, Phys. Rev. B **41**, 10 000 (1990); see also S. Schmitt-Rink, J. B. Stark, W. H. Knox, D. S. Chemla, and W. Schäfer, Appl. Phys. A: Solids Surf. **53**, 491 (1991) and the references therein.
[15] R. S. Knox, *Theory of Excitons, in Solid State Physics*, edited by H. Ehrenreich, F. Seitz, and D. Turnbull (Academic, New York, 1963), Suppl. 5, p. 207.
[16] L. P. Gor'kov and I. E. Dzyaloshinskii, Zh. Eksp. Teor. Fiz. **53**, 717 (1967) [Sov. Phys. JETP **26**, 449 (1968)].
[17] A. B. Dzyubenko and A. L. Yablonskii, Pis'ma Zh. Eksp. Teor. Fiz. **64**, 198 (1996) [JETP Lett. **64**, 213 (1996)].
[18] N. A. Gippius, A. B. Dzybenko, and S. G. Tikhodeev (to be published).
[19] J. Dreybrodt, A. Forchel, and J. P. Reithmaier, Phys. Rev. B **48**, 14 741 (1993).
[20] A maximum of E_{1s} at very small L_{cap} is due to the exciton binding energy decrease caused by the high vacuum potential, which pushes out the QW level from the well, when separation from vacuum becomes very small.
[21] C. Presilla, V. Emiliani, and A. Frova, Semicond. Sci. Technol. **10**, 577 (1995).
[22] T. B. Borzenko, Y. I. Koval, L. V. Kulik, and A. V. Larionov, Appl. Phys. Lett. **70** 2291 (1997).
[23] J. C. Maan, G. Belle, A. Fasolino, M. Altarelly, and K. Ploog, Phys. Rev. B **30**, 2253 (1984).
[24] G. E. W. Bauer and T. Ando, Phys. Rev. B **38**, 6015 (1988).
[25] I. V. Lerner and Yu. E. Lozovik, Zh. Eksp. Teor. Fiz. **78**, 1167 (1980) [Sov. Phys. JETP **51**, 588 (1980)].